CHINESE OPTICS LETTERS

Vol. 19, No. 10 | October 2021

Dual-frequency fringe for improving measurement accuracy of three-dimensional shape measurement

Zixiao Miao (苗自晓) and Qican Zhang (张启灿)*

Department of Opto-Electronics, Sichuan University, Chengdu 610065, China

*Corresponding author: zqc@scu.edu.cn

Received December 30, 2020 | Accepted March 18, 2021 | Posted Online August 9, 2021

A new phase unwrapping method based on dual-frequency fringe is proposed to improve both high accuracy and large measurement range of three-dimensional shape measurement by synthesizing the projected dual-frequency fringes obtaining higher and lower frequencies. The lower-frequency one is their phase difference, which can help unwrap the wrapped phase of the higher-frequency one from their phase sum. In addition, the relationship between the measuring accuracy and the frequencies of the projected fringes is studied to guide the frequency selection in actual measurement. It is found that the closer the two frequencies are, the higher the measurement accuracy will be. The computer simulation and experiment results show the viability of this method.

Keywords: fringe projection; 3D shape measurement; dual frequency; phase shifting; phase sum.

DOI: 10.3788/COL202119.102601

1. Introduction

Three-dimensional (3D) shape reconstruction has been widely used in the practical applications of modern information technology in machine design, industrial inspection, robotics, and game industry due to its high speed and high flexibility[1–6]. The fringe projection profilometry (FPP) technique is considered to be one of the most reliable methods for restoring the 3D shape of objects due to its efficiency[7–9]. The FPP technique is principally used to project the fringe patterns onto the target object and to capture the distorted fringe pattern(s) by an angled camera. Then, the corresponding wrapped phase can be recovered from the captured images by using different fringe analysis algorithms, which derived phase-shifting measurement profilometry (PMP)[10–12], Fourier transform profilometry (FTP)[13,14], etc. These methods extract the phase information of the measured object's height by using arctangent calculation. Therefore, the phase distribution is wrapped within the value range from $-\pi$ to π; sequentially, the phase unwrapping must be implemented to acquire a continuous phase map for accurate 3D shape reconstruction.

The phase unwrapping algorithms can be commonly classified into spatial phase unwrapping[15–17] and temporal phase unwrapping[18–21]. For spatial phase unwrapping, each single wrapped phase map of a measured object can be unwrapped in the spatial domain, which usually uses the phase relationship between adjacent pixels to obtain the unwrapped phase value. However, such spatial phase unwrapping algorithms have one common limitation: they tend to fail if the abrupt surface changes introduce more than 2π phase variation from one sampling point to the next. In contrast, the temporal phase unwrapping algorithm fundamentally tries to eliminate the limitation of spatial phase unwrapping by capturing more patterns. They can be used to analyze the highly discontinuous object because the unwrapping process is independent for each spatial point.

Among temporal phase unwrapping algorithms, one popular method is to use the dual-frequency (or wavelength) phase-shifting technique[22–24]. The projected fringe patterns with different frequencies are used to generate an equivalent phase map, φ_{eq}, whose frequency can be determined with the difference of f_1 and f_2, i.e., $f_{\mathrm{eq}} = f_1 - f_2$. Since the synthetic frequency is lower than both frequencies of the projected fringes, the measurement range depth can be extended. However, the measurement accuracy is reduced with the increasing noise and lower equivalent frequency phase.

The phase sum with high sensitivity in two-wavelength phase-metrology (TWPM) was proposed for the first time, to the best of our knowledge, by Mustafin and Seleznev in 1970[25], and then Di *et al.* applied phase sum in digital holography for improving the measurement accuracy[26,27]. Inspired by their study, combined with the superiority of the higher- and lower-frequency fringes by synthesizing the projected dual-frequency fringes, a method of 3D shape reconstruction based on dual-frequency fringes is proposed, in which large measurable depth and high measurement accuracy can be achieved simultaneously. The phase difference of the projected dual-frequency fringes is used to produce a wrapped phase with synthetic

lower-frequency information, which enlarges the range of the measurable depth. With the help of the phase difference, the unwrapped phase sum is obtained as the final measurement results. The unwrapped phase of synthetic higher-frequency information, which is extracted from the phase sum, can improve the measurement accuracy of the system. The simulation and experimental results verify the availability of this proposed method.

2. Principle

In 3D shape measurement using fringe structured light, the intensity of deformed fringes recorded by a digital camera can be given by

$$I_n(x,y)=R(x,y)\{A(x,y)+B(x,y)\cos[\phi(x,y)-2\pi n/N]\}, \quad (1)$$

where (x,y) is the pixel coordinate, $R(x,y)$ represents the uneven reflectivity of the tested object surface, $A(x,y)$ is the background intensity, $B(x,y)$ is the modulation intensity, N is the phase-shift index, $n=0,1,2,\ldots,N-1$, and the wrapped phase $\phi(x,y)$ reflects the height of the object information, which can be extracted by the following equation:

$$\phi(x,y)=\arctan\frac{\sum_{n=0}^{N-1}I_n(x,y)\sin(2\pi n/N)}{\sum_{n=0}^{N-1}I_n(x,y)\cos(2\pi n/N)}. \quad (2)$$

Since there are three unknowns, $A(x,y)$, $B(x,y)$, and $\phi(x,y)$, in Eq. (1), at least three images with different phase shifting should be used to calculate the wrapped phase $\phi(x,y)$.

The phase value provided from Eq. (2) contains 2π phase discontinuities. Its corresponding continuous phase distribution $\Phi(x,y)$ can be unwrapped as Eq. (3):

$$\Phi(x,y)=\phi(x,y)+2k\pi, \quad (3)$$

where k is the integer number to indicate the fringe orders.

As shown in Fig. 1, in 3D shape measurement based on dual-frequency fringes, two projected fringes with different frequencies, f_h and f_l, are projected to obtain their corresponding wrapped phase ϕ_h and ϕ_l by Eq. (2). The basic process of this dual-frequency method is to subtract the wrapped phase ϕ_l from ϕ_h, sum the wrapped phase ϕ_h and ϕ_l, and then adjust the results to be within the range of $[0,2\pi]$:

$$\phi_d(x,y)=\begin{cases}\phi_h(x,y)-\phi_l(x,y), & \text{if } \phi_h\geq\phi_l,\\ \phi_h(x,y)-\phi_l(x,y)+2\pi, & \text{if } \phi_h<\phi_l,\end{cases}$$
$$\phi_s(x,y)=\begin{cases}\phi_h(x,y)+\phi_l(x,y), & \text{if } \phi_h+\phi_l\geq 0,\\ \phi_h(x,y)+\phi_l(x,y)+2\pi, & \text{if } \phi_h+\phi_l<0,\end{cases} \quad (4)$$

where ϕ_d and ϕ_s represent the phase difference and phase sum. Their corresponding lower (f_d) and higher (f_s) equivalent frequencies are defined as

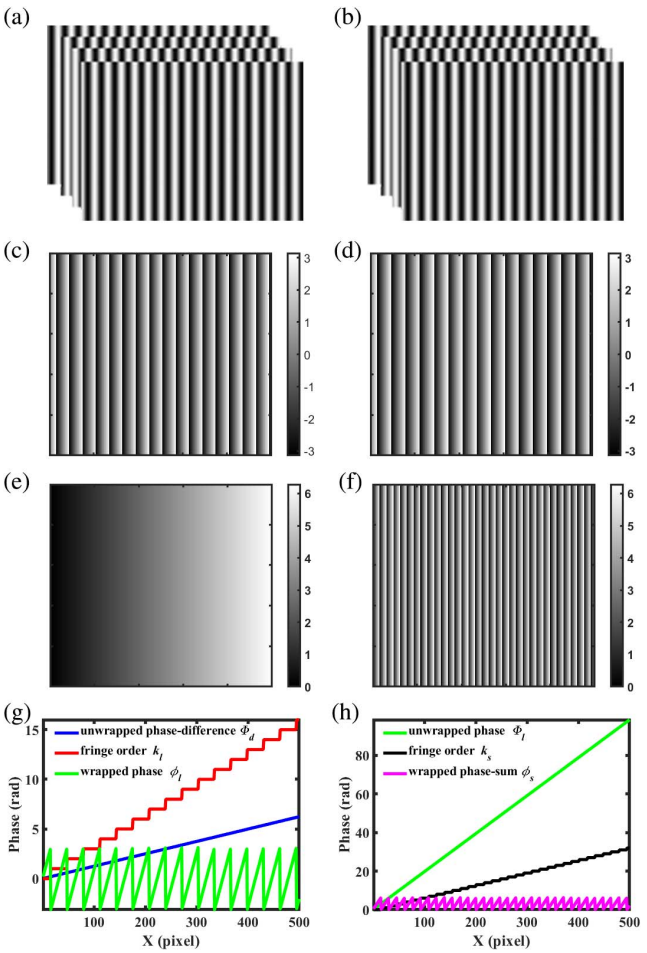

Fig. 1. Principle of the proposed dual-frequency method: (a) four phase-shifting patterns of f_h; (b) four phase-shifting patterns of f_l; (c) wrapped phase ϕ_h; (d) wrapped phase ϕ_l; (e) phase difference ϕ_d; (f) phase sum ϕ_s; (g) one cross section of the unwrapped phase difference Φ_d, fringe order k_l, and wrapped phase ϕ_l; (h) one cross section of the phase sum ϕ_s, fringe order k_s, and unwrapped phase Φ_l.

$$f_d=f_h-f_l, \quad f_s=f_h+f_l. \quad (5)$$

If the phase-difference map ranging from 0 to 2π covers the whole range of the surface, phase unwrapping is not necessary because ϕ_d can be regarded as the unwrapped phase, i.e., $\Phi_d=\phi_d$. Φ_d can be used to obtain the fringe order for each point on the low-frequency f_l wrapped phase for phase unwrapping. We choose the low frequency f_l rather than the high frequency f_h, which is to reduce the phase unwrapped order errors caused by noise amplification.

The fringe order k_l of ϕ_l is

$$k_l=\text{round}\left(\frac{\Phi_d\cdot f_l/f_d-\phi_l}{2\pi}\right), \quad (6)$$

where round $(\cdot)$ is the operator that gives the nearest integer number.

This results in the unwrapped phase of f_l, which is given by

$$\Phi_l(x,y) = \phi_l(x,y) + 2\pi \cdot k_l(x,y). \tag{7}$$

The fringe order k_s of ϕ_s is

$$k_s = \text{round}\left(\frac{\Phi_l \cdot f_s/f_l - \phi_s}{2\pi}\right). \tag{8}$$

This results in the unwrapped phase of f_s, which is given by

$$\Phi_s(x,y) = \phi_s(x,y) + 2\pi \cdot k_s(x,y). \tag{9}$$

The measured object's absolute phase map can be obtained by subtracting the phase of the reference plane from the unwrapped phase in the phase-sum information.

The synthetic frequency information and their phases depend on the frequencies of the projected fringes. By selecting the appropriate fringe's frequency, the synthetic frequency will change accordingly. The phase difference extends the range of measurable depth variation by the synthetic lower frequency. In addition, the synthetic phase sum has an averaging effect in the process of calculating the synthetic frequency and thus smoothing the phase noise.

In order to illustrate the relationship of phase difference with phase sum, the sensitivity gain G is defined as

$$G = \frac{f_h + f_l}{f_h - f_l}. \tag{10}$$

That is, the phase sum is G times more sensitive than the phase difference. The purpose of using phase difference is to synthesize a lower frequency f_d. In other words, if the phase difference is meaningful, the phase-difference frequency must be lower than the original low frequency of f_l, so it is necessary that

$$f_d = f_h - f_l < f_l \Rightarrow f_h < 2f_l \Rightarrow G = \frac{f_h + f_l}{f_h - f_l} > 3. \tag{11}$$

However, the synthesis fringes corresponding to the phase difference should cover the whole measurement area, which means that the two projected frequencies are close to each other, and G is much larger than three. The measurement accuracy increases with the increasing sensitivity gain G. Therefore, the value of G can be used to guide the selection of frequency.

3. Computer Simulation

We simulated 3D shape measurement by using FPP for a tested object whose shape distribution acts like the peaks function. The diagram of the computer simulation process of this work is shown in Fig. 2. The process of phase unwrapping uses the phase difference ϕ_d to help the phase-sum ϕ_s unwrapping.

The continuous phase is 500×500 pixels. The frequency of a projected fringe pattern is actually defined as $1/T$ in an FFP system, where T is the number of pixels in each period. According

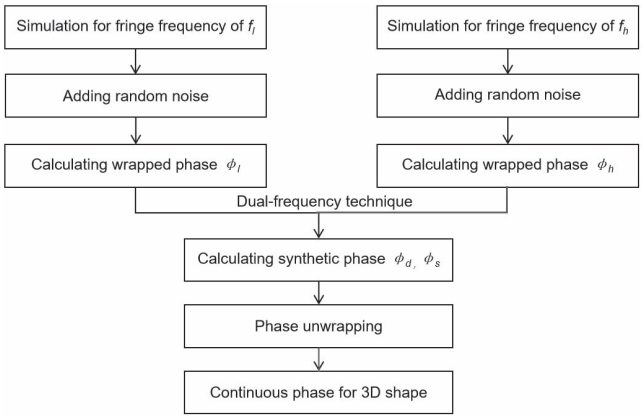

Fig. 2. Chart of the computer simulation process of the proposed dual-frequency by FPP.

to Eq. (5), both of the original fringe frequencies f_l and f_h ($T_l = 170$ pixels, $T_h = 150$ pixels) are lower than the synthetic frequency f_s ($T_s = 79.7$ pixels). Taking the data along 250th row as an example, the wrapped phase, the unwrapped phase, the object's height, and the height error are plotted in Fig. 3. The phase differences are shown in Fig. 3(a), and the phase sum is shown in Fig. 3(b). Figures 3(c) and 3(d) show the process of the phase unwrapping.

In order to compare the performance of the proposed method, a random Gaussian noise with a signal-to-noise ratio (SNR) of 27 dB is designed to be added in the simulated fringes, and all of the phase distributions have been transformed to the height distribution. Figure 3(e) shows the cross section along one row of the restored object's height. Related to the simulated object's truth shape, the corresponding height errors restored by two original projected fringes and the synthetic fringes were analyzed, and their cross sections along one row are shown in Fig. 3(f). Due to the higher synthetic frequency and denser wrapped phase fringes, we can see that the noise of the synthetic frequency's restored height (magenta line) is obviously smaller than that of the other two. The standard deviation (STD) of the synthetic frequency's height error distribution is 0.325, while those of f_l and f_h are 0.490 and 0.433, respectively. In effect, the noise is reduced by the superimposing operations in the process of calculating the synthetic wrapped phase. Therefore, the measurement accuracy can be increased with this proposed dual-frequency technique.

In this simulation, the phase sensitivity gain G between the phase sum and phase difference is given by

$$G = \frac{f_h + f_l}{f_h - f_l} = \frac{1/150 + 1/170}{1/150 - 1/170} = 16. \tag{12}$$

To confirm the relationship between the sensitivity gain G and the measurement accuracy, we carried out simulation by selecting a fixed high frequency of 1/30 and changed the low frequency from 1/31 to 1/125. Figure 4 shows the trend of measurement accuracy changing with the low frequency.

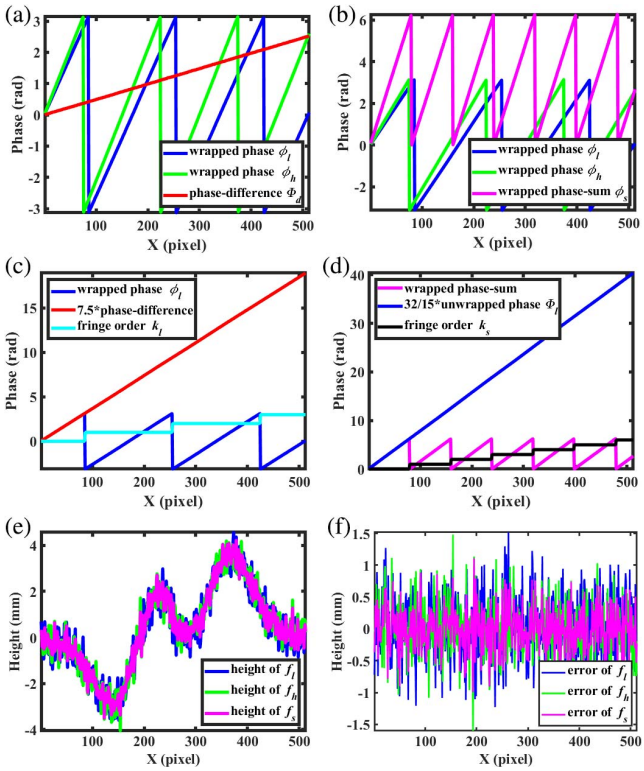

Fig. 3. Computer simulation results of the proposed dual-frequency in 3D shape measurement. (a), (b) One cross section of wrapped phases (T_l = 170 pixels, T_h = 150 pixels) and synthetic phases (T_d = 1275 pixels, T_s = 79.7 pixels); (c) one cross section of wrapped phase ϕ_h, phase difference ϕ_d, and fringe order k_l; (d) one cross section of wrapped phase ϕ_s, unwrapped phase Φ_l, and fringe order k_s; (e) one cross section of the restored object's height; (f) one cross section of the restored height error.

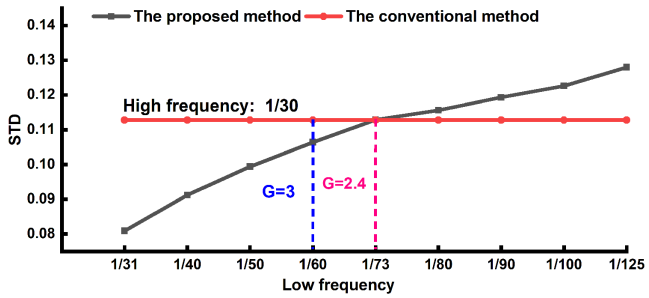

Fig. 4. Trend chart of measurement accuracy with the high frequency of 1/30 and changing low frequency.

It is clear that the accuracy is the best when the dual-frequency fringes are close to each other. We conclude that the effect of phase sum for improving accuracy relies on the ratio of f_s to f_d. As can be seen from the figure, the phase sum is not meaningful after the intersection of two lines. Therefore, we find G is approximately 2.4 at the intersection. From the above, it is meaningful to use dual-frequency fringe for $G > 3$. At the point of $G = 3$, the accuracy of the proposed method is higher than that of the conventional method. Therefore, the phase sum in the dual-frequency technique can obviously improve the measurement accuracy.

4. Experimental Results

To further verify the performance of the proposed method, we developed an FFP system including a projection system [digital projector with a digital light processing (DLP) chip and the resolution of 800 × 1280 pixels], imaging equipment (UI-3250CP-M-GL camera with the resolution of 1200 × 1600 pixels), and a computer. The distance between the projector and the camera was about 200 mm. The measured objects were placed at around 500 mm in front of the FFP system, where a flat board was used as the reference plane. Fringe patterns were generated and then projected onto the tested surface. Afterward, the deformed fringe patterns were captured by the camera.

In our experiments, the absolute phase calculated by a 24-step phase-shifting algorithm is used as the ground truth. It should be noted that all of the images have been cropped according to the tested object in the following illustrations. In these experiments, we compared the 3D reconstruction accuracy of the proposed method with that of the conventional dual-frequency method reported in literature [24]. In order to verify the proposed method, the reference plane was first measured, and the reconstruction phase error is shown in Fig. 5. The measurement accuracy of the conventional dual-frequency method is mainly determined by the high frequency of two projected fringes, so it

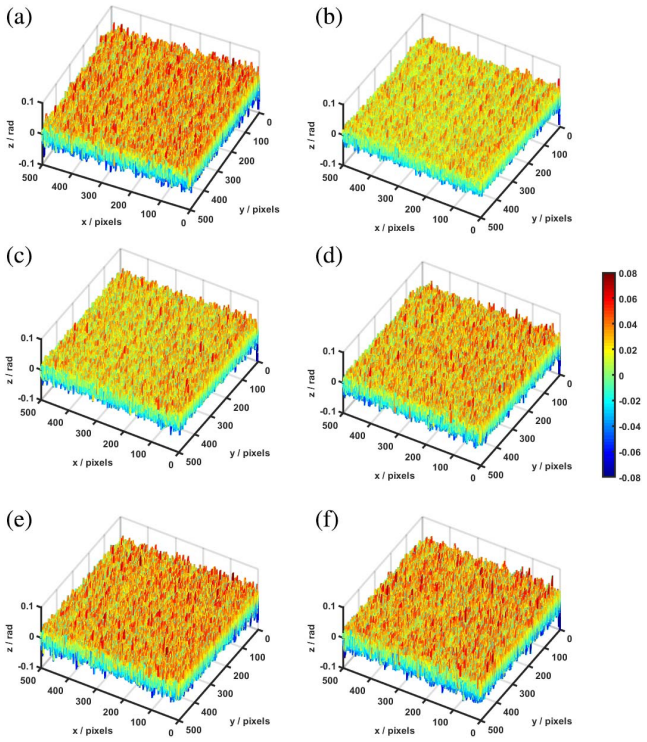

Fig. 5. Reconstruction phase error of reference plane (a) by the conventional dual-frequency method and (b)–(f) by the proposed dual-frequency method with different low frequencies (f_h = 1/45, and f_l = 1/50, 1/70, 1/90, 1/120, 1/140).

will not be improved even though the low-frequency fringe is changing. The STD of the conventional dual-frequency method is 0.0165, while the STD of the proposed dual-frequency method is, respectively, 0.0130, 0.0143, 0.0154, 0.0164, and 0.0170 with the increasing T_l.

Then, one simple object with a smooth surface and one complex object were measured. The unwrapped phase was obtained to reconstruct the 3D shape of the measured object. Figures 6(a) and 6(b) show one of the captured fringe patterns with very close spatial frequencies having $T_h = 80$ pixels and $T_l = 85$ pixels. Figures 6(c) and 6(d) show the wrapped phase of the projected dual-frequency fringes. Figures 6(e) and 6(f), respectively, present the information of phase difference and phase sum. Figure 6(g) presents the fringe order k_l. After applying Eq. (7), the unwrapped phase Φ_l is retrieved, as shown in Fig. 6(h). Figure 6(i) presents the fringe order k_s, and the unwrapped phase Φ_s is retrieved by Eq. (9) and shown in Fig. 6(j). The phase sensitivity gain G between the phase sum and phase difference is given by

$$G = \frac{f_h + f_l}{f_h - f_l} = \frac{1/80 + 1/85}{1/80 - 1/85} = 33. \tag{13}$$

In order to research the relationship between the sensitivity gain G and the measurement accuracy, a series of experiments were carried out. The second experiment was carried out on a complex object with the projected fringes of $T_h = 45$ pixels and $T_l = 50$, 70, 90, 120, and 140 pixels. Figure 7 illustrates the 3D reconstruction results, where the first one gives the 3D shape reconstructed by the conventional method, and the others are the 3D shapes reconstructed by our proposed method with different lower-frequency fringes. Meanwhile, to show their difference more clearly, the corresponding errors related to the absolute phase, which were calculated by the 24-step phase-shifting algorithm, have also been calculated and shown in Fig. 8. The STD of the conventional dual-frequency method is 0.0234, while the STD of the proposed dual-frequency method is, respectively, 0.0187, 0.0202, 0.0217, 0.0235, and 0.0241 with the increasing T_l.

Figure 9 is a trend chart of measurement accuracy of actual experiments with a fixed high frequency and a varied low frequency. The measured object in Fig. 9(a) is the foam heart in the first experiment scene, and the measured object in Fig. 9(b) is the petal in the second experiment scene. It is obvious that the phase error becomes larger as the frequency difference between the two original fringes increases. It can also be concluded that the higher the sensitivity gain G, the higher the measuring accuracy.

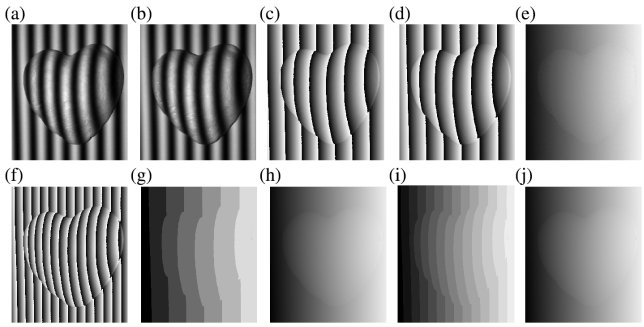

Fig. 6. Experimental results of measuring a simple object: (a), (b) one of the captured fringe patterns of f_h and f_l (T_h = 80 pixels, T_l = 85 pixels); (c), (d) wrapped phases ϕ_h and ϕ_l; (e) phase difference (T_d = 1360 pixels); (f) wrapped phase sum (T_s = 41.2 pixels); (g) fringe order k_l; (h) unwrapped phase Φ_l; (i) fringe order k_s; (j) unwrapped phase sum Φ_s.

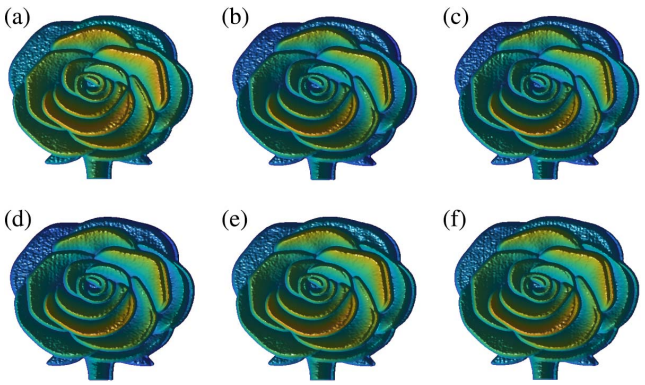

Fig. 7. Reconstruction of the object's absolute phase (a) by the conventional dual-frequency method and (b)–(f) by the proposed dual-frequency method with different low frequencies (f_h = 1/45, and f_l = 1/50, 1/70, 1/90, 1/120, 1/140).

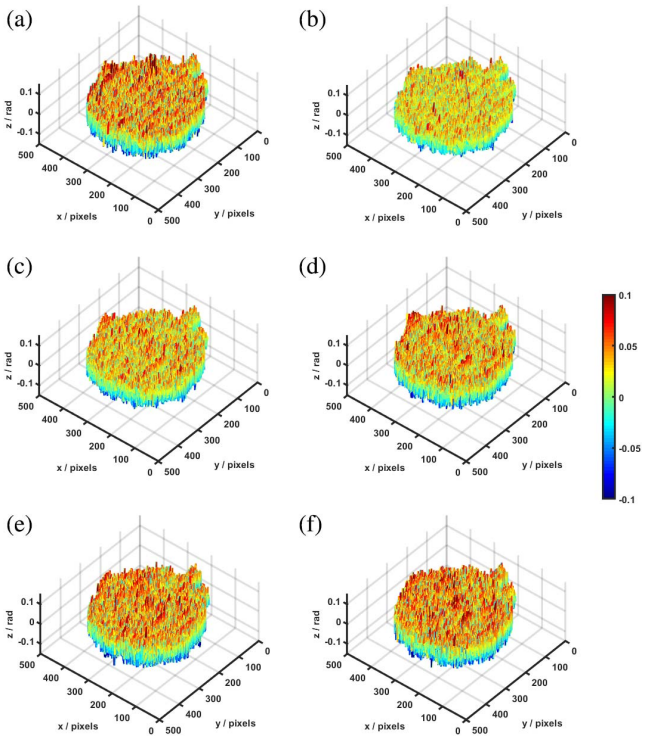

Fig. 8. Reconstruction phase errors with different low frequencies corresponding to Fig. 7.

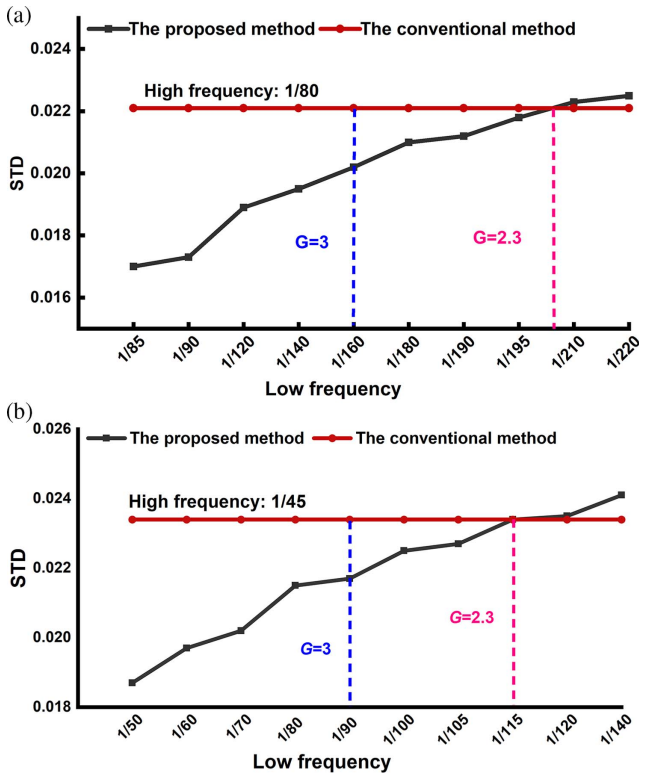

Fig. 9. Trend chart of measurement accuracy of actual experiments with a fixed high frequency and various low frequencies in measuring (a) the foam heart and (b) the petal.

However, there will be many interference factors in the actual experiment, such as the nonlinear error of the projector, uneven reflectivity of the object surface, camera resolution, shadow, environmental light, etc. It can be seen from the phase error distribution that it is obviously periodic, which is mainly caused by the nonlinear error of the projector. The experimental results are not as accurate as the simulation ones, but the trend is basically the same. At the point of $G = 3$, the measuring accuracy of the proposed method is higher than that of the conventional method, which verifies that the phase sum in dual-frequency method can improve the measuring accuracy.

5. Conclusion

In this study, a dual-frequency method in 3D measurement is certified to enhance the measurement accuracy. Compared with the conventional dual-frequency method, the proposed dual-frequency method employs the phase sum of two different frequency projected fringes to improve the measuring accuracy. A synthetic fringe is acquired, which is higher in frequency than either of the original projected fringes. The measurement results with the synthetic fringes are superior to that of a single frequency fringe, and higher measurement accuracy is also obtained. In addition, the relationship between the sensitivity gain G and the measurement accuracy is also studied to guide the frequency selection in actual measurements. We found that the larger the sensitivity gain G is, the higher the measurement accuracy will be. Especially, when $G = 3$, the measurement accuracy of the proposed method is also higher than that of the conventional method. Both the computer simulation and actual experimental results demonstrate the viability of the proposed method.

Acknowledgement

This work was supported by the National Natural Science Foundation of China (No. 62075143).

References

1. F. Chen, G. Brown, and M. Song, "Overview of 3-D shape measurement using optical methods," Opt. Eng. **39**, 10 (2000).
2. X. Su and Q. Zhang, "Dynamic 3-D shape measurement method: a review," Opt. Lasers Eng. **48**, 191 (2010).
3. S. Zhang, "High-speed 3D shape measurement with structured light methods: a review," Opt. Lasers Eng. **106**, 119 (2018).
4. C. Zuo, S. Feng, L. Huang, T. Tao, W. Yin, and Q. Chen, "Phase shifting algorithms for fringe projection profilometry: a review," Opt. Lasers Eng. **109**, 23 (2018).
5. L. Li, Z. Pan, H. Cui, J. Liu, S. Yang, L. Liu, Y. Tian, and W. Wang, "Adaptive window iteration algorithm for enhancing 3D shape recovery from image focus," Chin. Opt. Lett. **17**, 061001 (2019).
6. J. Dai, L. Huang, K. Guo, L. Ling, and H. Huang, "Reflectance transformation imaging of 3D detection for subtle traces," Chin. Opt. Lett. **19**, 013501 (2021).
7. S. Zhang, "High-resolution 3D profilometry with binary phase-shifting methods," Appl. Opt. **50**, 1753 (2011).
8. S. Zhang, D. Weide, and J. Oliver, "Superfast phase-shifting method for 3-D shape measurement," Opt. Express **18**, 9684 (2010).
9. C. Zuo, Q. Chen, S. Feng, G. Gu, and A. Asundi, "Real-time three-dimensional infrared imaging using fringe projection profilometry," Chin. Opt. Lett. 11, S21101 (2013).
10. V. Srinivasan, H. Liu, and M. Halioua, "Automated phase-measuring profilometry of 3-D diffuse objects," Appl. Opt. **23**, 3105 (1984).
11. X. Su, G. Bally, and D. Vukicevic, "Phase-stepping grating profilometry: utilization of intensity modulation analysis in complex objects evaluation," Opt. Commun. **98**, 141 (1993).
12. S. Zhang and S. T. Yau, "High-resolution, real-time 3D absolute coordinate measurement based on a phase-shifting method," Opt. Express **14**, 2644 (2006).
13. M. Takeda, H. Ina, and S. Kobayashi, "Fourier-transform method of fringe-pattern analysis for computer-based topography and interferometry," J. Opt. Soc. Am. A **72**, 156 (1982).
14. X. Su and W. Chen, "Fourier transform profilometry: a review," Opt. Lasers Eng. **35**, 263 (2001).
15. R. Goldstein, H. Zebker, and C. Werner, "Satellite radar interferometry: two-dimensional phase unwrapping," Rad. Sci. **23**, 713 (1988).
16. T. Flynn, "Two-dimensional phase unwrapping with minimum weighted discontinuity," J. Opt. Soc. Am. A **14**, 2692 (1997).
17. X. Su and W. Chen, "Reliability-guided phase unwrapping algorithm: a review," Opt. Lasers Eng. **42**, 245 (2004).
18. J. Huntley and H. Saldner, "Temporal phase-unwrapping algorithm for automated interferogram analysis," Appl. Opt. **32**, 3047 (1993).
19. Y. Cheng and J. Wyant, "Two-wavelength phase shifting interferometry," Appl. Opt. **23**, 4539 (1985).
20. V. Gushov and Y. Solodkin, "Automatic processing of fringe patterns in integer interferometers," Opt. Lasers Eng. **14**, 311 (1991).
21. C. Zuo, L. Huang, M. Zhang, Q. Chen, and A. Asundi, "Temporal phase unwrapping algorithms for fringe projection profilometry: a comparative review," Opt. Lasers Eng. **85**, 84 (2016).
22. K. Creath, "Step height measurement using two-wavelength phase-shifting interferometry," Appl. Opt. **26**, 2810 (1987).

23. D. Towers, J. Jones, and C. Towers, "Optimum frequency selection in multi-frequency interferometry," Opt. Lett. **28**, 887 (2003).
24. J. Hyun and S. Zhang, "Enhanced two-frequency phase-shifting method," Appl. Opt. **55**, 4395 (2016).
25. K. S. Mustafin and V. A. Seleznev, "Methods of increasing the sensitivity of holographic interferometry," Sov. Phys. Uspekhi **13**, 416 (1970).
26. J. Di, W. Qu, B. Wu, X. Chen, J. Zhao, and A. Asundi, "Dual wavelength digital holography for improving the measurement accuracy," Proc. SPIE **8769**, 87690G (2013).
27. J. Di, J. Zhang, T. Xi, C. Ma, and J. Zhao, "Improvement of measurement accuracy in digital holographic microscopy by using dual-wavelength technique," J Micro/Nanolithogr. MEMS, MOEMS **14**, 041313 (2015).